In vitro mesenchymal stem cell response to a CO_2 laser modified polymeric material

D.G. Waugh [a,*], I. Hussain [b], J. Lawrence [a], G.C. Smith [a], D. Cosgrove [b], C. Toccaceli [a]

[a] Laser Engineering and Manufacturing Research Centre, Faculty of Science and Engineering, University of Chester, Chester CH1 4BJ, UK
[b] School of Life Sciences, Brayford Pool, University of Lincoln, Lincoln LN6 7TS, UK

ABSTRACT

With an ageing world population it is becoming significantly apparent that there is a need to produce implants and platforms to manipulate stem cell growth on a pharmaceutical scale. This is needed to meet the socio-economic demands of many countries worldwide. This paper details one of the first ever studies in to the manipulation of stem cell growth on CO_2 laser surface treated nylon 6,6 highlighting its potential as an inexpensive platform to manipulate stem cell growth on a pharmaceutical scale. Through CO_2 laser surface treatment discrete changes to the surfaces were made. That is, the surface roughness of the nylon 6,6 was increased by up to 4.3 μm, the contact angle was modulated by up to 5° and the surface oxygen content increased by up to 1 atom %. Following mesenchymal stem cell growth on the laser treated samples, it was identified that CO_2 laser surface treatment gave rise to an enhanced response with an increase in viable cell count of up to 60,000 cells/ml when compared to the as-received sample. The effect of surface parameters modified by the CO_2 laser surface treatment on the mesenchymal stem cell response is also discussed along with potential trends that could be identified to govern the mesenchymal stem cell response.

© 2016 Elsevier B.V. All rights reserved.

1. Introduction

Surface treatments such as radiation grafting [1], plasma surface modification [2,3] and the implementation of various coatings [4] in biological applications are becoming more widely used within science and industry. These surface treatments possess the ability to enhance surface properties and, from a bioengineering perspective, enhance the biofunctionality of the material [5–7]. This is significant as, on numerous occasions, the surface properties of a material give rise to a biological cell response which is insufficient leading to rejection of the material. This results in minimal, or no, biological adhesion taking place. By manipulating the surfaces of these materials to be more biomimetic the cell response can be greatly enhanced, reducing the rejection rates of biological environments to foreign objects (metals, ceramics and polymers). What is more, there is a considerable increase in interest from industry to develop substrates and scaffolds upon which human tissue can be efficiently grown and then implanted into the human body. The interest from industry in producing platforms for pharmaceutical scale human tissue production will ultimately remove the need for foreign objects as implantable materials. This will ultimately lead to industry considering and taking up inexpensive polymeric materials for

large-scale pharmaceutical production, removing the demand for comparatively expensive metal/ceramic alternatives.

Compared to alternative techniques, laser surface treatment has been shown to have the ability to modify the surface of a material, making discrete changes to the surface topography and surface chemistry, simultaneously [8–12]. Further advantages over competing techniques to be gained from the implementation of lasers for surface treatments are:

- Accuracy, precision and repeatability of material processing;
- Non-contact processing offering a somewhat clean manufacturing technique, requiring minimal post-processing;
- Discrete modifications to the surface without affecting the bulk properties.

Mesenchymal stem cells (MSCs) are extremely important for the development and regeneration of mesenchymal tissues [13–16]. As such, MSCs, which are currently subject to significant scientific research, have been found to differentiate into specialized cell types (such as osteoblasts, chondrocytes, tenocytes, etc.) [17]. This demonstrates how MSCs have become the most promising cell type for tissue engineering and regenerative medicine. Recent evidence suggests that material platforms/substrates to mimic a natural niche environment offer a significant engineering approach to prolong the in vitro lifespan of MSCs while still maintaining their multipotency [18–21]. With this in mind,

for tissue engineering applications, MSCs are commonly grown on scaffolds of biomaterial which are carefully designed to provide both structural support and a substrate for cellular adhesion [20,22]. An important finding was made by Curtis and Wilkinson [22] who stated that cells are able to discriminate among subtle differences in surface roughness and topography, resulting in different protein adsorption and cellular responses of morphology, differentiation, proliferation, and orientation. This research therefore highlights the advantages of manipulating cells by implementing specific surface treatments.

Previous studies with MSCs have indicated that they are sensitive to surface roughness and topography of the material on which they are growing [23,24]. For instance, Kommireddy et al. [21] reported that cell attachment of MSCs is affected by the surface roughness and increased cell attachment is found on the rougher surface than the smoother surfaces. In a similar manner, Myllymaa et al. [20] found that MSCs are sensitive to the topographical variations and is likely to interact with the physical environment by aligning its orientation along the physical shape and edges. This also corresponds with research which has been carried out previously with osteoblast cells [25–27]. On account of the evidence in the literature for the manipulation of biological cells by modifying the surface of the substrate/platform, laser surface treatment lends itself to be an attractive means to provide an optimized surface for the manipulation of MSC growth and differentiation.

On account of the significance of the topography and surface chemistry on MSC response this paper details one of the first ever investigations in to the response of MSCs to CO_2 laser-induced patterning of nylon 6,6. The biocompatibility and cell response upon laser textured polymer is discussed, offering an inexpensive and effective technique in comparison to conventional biomaterial scaffold materials and technology.

2. Experimental technique

2.1. Material

The nylon 6,6 was sourced in 100 mm × 100 mm sheets with a thickness of 5 mm (Goodfellow Cambridge, Ltd., UK). The nylon 6,6 was mechanically cut into 10 mm diameter samples for CO_2 laser processing, topography analysis, surface chemistry analysis and wettability analysis. Smaller samples with a diameter of 5 mm were mechanically cut for the biological analysis.

2.2. CO_2 laser material processing

The CO_2 laser (60 W ti-series; Synrad Inc.; USA), together with Synrad Winmark software version 6 were used to generate the required patterns on the surface of the samples. The laser head of the system was 195 mm away from the sample, which gave rise to a 95 μm spot size. It should also be noted that the target material and laser system were held in a laser safety cabinet in which the ambient gas was air. Furthermore, an extraction system was used to remove any fumes produced during laser processing. The laser-induced patterns were trenches with 50 μm spacing (CT50), hatch with 50 μm spacing (CH50), trenches with 100 μm spacing (CT100) and hatch with 100 μm spacing (CH100). In addition, an as-received control sample was used (AR). The applied scan strategies implemented can be seen in Fig. 1. For each of the irradiated patterns the laser power was kept constant at 11.7% (7 W) with a scanning speed of 600 mm s^{-1}. For each of the experiments the fluence was calculated to be 16 Jcm^{-2} and the irradiance was calculated to be 99 kW cm^{-2}.

The laser processed percentage area for the trench and hatch patterns were calculated. For the trench pattern processed area, %A$_t$, where the laser beam scanned lines did not overlap (sample CT100)
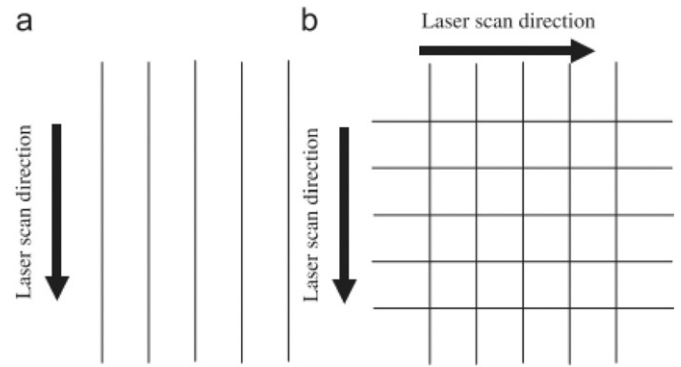

Fig. 1. Diagram showing the scan strategy implemented for (a) the trench and (b) hatch CO_2 laser-induced patterning.

Eq. (1) was used.

$$\%A_t = \frac{A_T}{A_S} = \frac{(N_L \cdot A_L)}{A_S} \tag{1}$$

where A_T is the laser-treated area, A_S is the total sample area, N_L is the number of laser scanned lines and A_L is the total area of the laser scanned lines. The non-treated percentage area was then calculated by deducting the calculated value from Eq. (1) from 100% of the total area.

For the trench patterned sample CT50, where the laser beam scanned lines did overlap due to the size of the spot size, Eq. (2) was used to determine the double area coverage, %A$_{to}$.

$$\%A_{to} = \frac{A_T}{A_S} = \frac{(N_L \cdot A_{LO})}{A_S} \tag{2}$$

where A_{LO} is the total area of the laser scanned lines also taking in to account the overlapping areas due to the spot size being larger than the distance between the scanned lines. As the whole surface area was processed with sample CT50, the amount of single area coverage was calculated by deducting the value obtained from Eq. (2) from 100% of the total area.

In order to calculate the area coverage values for the hatch patterns the samples were split in to squares as shown in Fig. 2.

Taking sample CH100 into account, the double percentage area coverage, %A$_{dc}$, of the sample was calculated using Eq. (3).

$$\%A_{dc} = \frac{2A_T}{A_S} = \frac{(N_{SQ} \cdot 2A_T)}{A_S} \tag{3}$$

where, N_{SQ} is the number of squares (Fig. 1) which included laser processing. For the non-treated percentage area, %A$_{NT}$, Eq. (4) was implemented.

$$\%A_{NT} = \frac{A_{NT}}{A_S} = \frac{(N_{SQ} \cdot A_{NT})}{A_S} \tag{4}$$

where A_{NT} is the non-laser treated area. The single area coverage of the laser scanned lines was ten calculated by deducting the values obtained from Eq. (3) and Eq. (4) from 100% of the total sample surface area.

For sample CH50, the quadruple percentage area coverage, %A$_Q$, was calculated using Eq. (5).

$$\%A_Q = \frac{4A_T}{A_S} = \frac{(N_{SQ} \cdot A_{LO})^2}{A_S} \tag{5}$$

The double percentage area coverage for sample CH50 was calculated using Eq. (3). The triple percentage area coverage was calculated by deducting the values obtained from Eq. (3) and Eq. (5) from 100% of the total surface area. It should be noted that, due to the laser spot size being
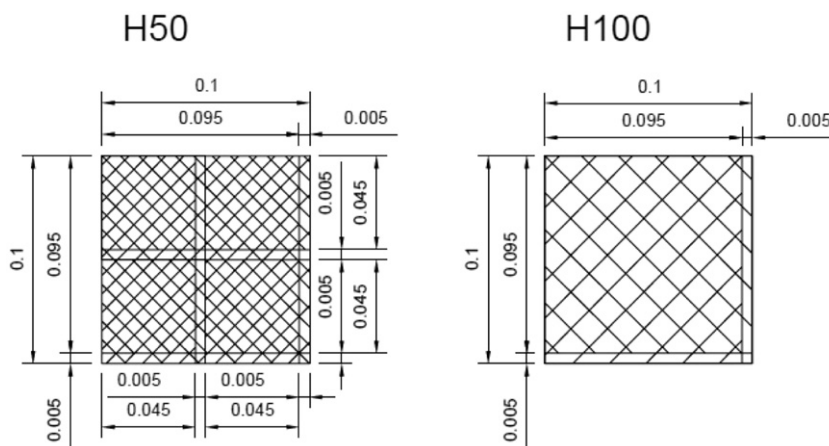
H50   H100

Fig. 2. Schematic diagrams of the CH50 and CH100 samples and how they were split in to squares for the calculation of the laser-scanned line area coverage.

larger than the scan line spacing for sample CH50, there was no single percentage area coverage and no untreated areas. The incident energies on each sample were determined by multiplying the laser processed surface areas by the measured fluence of 16 J cm^{-2}.

2.3. Topography analysis

The surface profiles of each sample were determined using a non-contact confocal chromatic imaging (CCI) system (Micromesure 2; STIL S.A.; France) with Surface Map software and TMS Plus software. The 3-D CCI profiler was set up using a 400 μm resolution probe at a working distance of 12 mm. On account of the software employed, Sa and Ra roughness parameters were determined for each sample. Ra can be defined as the arithmetic average of the absolute values along a single specified direction and Sa the arithmetic average of the absolute values over the whole of the laser surface treated area.

2.4. Wettability analysis

In accordance with Rance, [28], a sessile drop device (goniometer OCA20; DataPhysics Instruments GmbH, Germany) was used with SCA20 software to allow the contact angle, θ, for triply distilled water and diiodomethane to be determined for each sample. Before measurement, the samples were cleaned using ethanol in an ultrasonic bath for 10 min. Following this the samples were air dried for 30 min. An average droplet volume of 5 μl implemented for the measurement of the distilled water, while for the diiodomethane the average droplet volume was 1 μl in order to provide a sufficient droplet to take measurements. By using the data obtained for the contact angles of the water and the diiodomethane, the two fluid Owens, Wendt, Rabel and Kaelble (OWRK) method [9,29] was used to determine the surface fee energy for each of the samples.

2.5. X-ray photoelectron spectroscopy (XPS) analysis

The XPS data were acquired using a bespoke ultra-high vacuum system fitted with a Specs GmbH Focus 500 monochromated Al Kα X-ray source, Specs GmbH Phoibos 150 mm mean radius hemispherical analyser with 9-channeltron detection, and a Specs GmbH FG20 charge neutralising electron gun. Survey spectra were acquired over the binding energy range 1100–0 eV using a pass energy of 50 eV and high resolution scans were made over the C1 s and O 1 s lines using a pass energy of 15 eV. Under these conditions the full width at half maximum of the Ag 3d$_{5/2}$ reference line is ~0.7 eV. In each case, the analysis was an area-average over a region approximately 2 mm in diameter on the sample surface. The energy scale of the instrument is calibrated according to ISO standard 15472, and the intensity scale is calibrated using an

in-house method traceable to the UK National Physical Laboratory [30]. Data were quantified using Scofield cross sections corrected for the energy dependencies of the electron attenuation lengths and the instrument transmission. Data interpretation was carried out using CasaXPS software v2.3.16.

2.6. Biological analysis

All cell culture procedures were performed under sterile conditions within a Class II Microbiological Safety Cabinet and research laboratory safety protocol was followed. All used items were correctly discarded in accordance with the laboratory safety protocol. Mesenchymal stem cells (MSCs) used in this study were from human umbilical cord blood (Stem Cell Bank, Japan). The primary MSCs used were at passage number 6. MSCs were grown in tissue culture medium consisting of Dulbecco's Modified Eagles Media (DMEM) (with L-glutamine) (Sigma Aldrich, Ltd.), supplemented with 10% fetal calf serum (FCS) (Sigma Aldrich, Ltd.), and 100 units/ml of penicillin and 0.1-mg/ml of streptomycin (Sigma Aldrich, Ltd.), and placed in an incubator set at 37 °C, 5% humidified CO2 (Wolf Laboratories, Ltd.), throughout the study. When the cells reached sub-confluent (70 to 80%), they were retrieved with 0.25% trypsin and 0.02% EDTA (Sigma Aldrich, Ltd.). The retrieved cells were washed twice with Phosphate buffer saline (PBS), centrifuged at 1200 rpm for 12 min at room temperature and re-seeded onto the samples which had been placed in the 24- and 96-well plates (Corning Costar). A consistent size of sample of 5×10^4 cell/ml was used throughout the in-vitro experiments.

The cell morphology on different samples after 24, and 48 h of culture was analyzed in the secondary electron (SE) mode by the SEM. The following procedure was undertaken to produce a sample that was dehydrated ready for Au coating. After removal of the culture media, the samples were initially rinsed with PBS (Sigma-Aldrich, Ltd.) to remove any unattached cells and then adherent cells were fixed using 1.2% glutaraldehyde in water (Sigma-Aldrich, Ltd.) at room temperature for an hour within the BSC. After an hour, the glutaraldehyde solution was removed and the fixed cells were washed with PBS prior to carrying out a graded series of ethanol/distilled water mixtures of 50%, 80%, 90%, 95%, 98% and 100%. Each sample was left in these mixtures for 10 min and dried in air. The samples were sputter coated with Au for cell morphology observation by SEM.

2.6.1. Cell counting

To ensure that the MSCs were prepared for counting, the MSCs were retrieved with 0.25% trypsin and 0.02% EDTA (Sigma Aldrich, Ltd.) The amount of viable cells on different samples after 24 h and 48 h of culture was counted in a 16 square of the haemocytometer (Neubauer Improved Bright Line at depth 0.1 mm, 0.00025 mm^3). Prior to counting,

cells were stained with trypan blue to illustrate the proportion of dead cells compared to living one and to aid in counting. 50 μl of homogeneous cell suspension with tissue culture medium comprised of DMEM supplemented with L-glutamine (Sigma Aldrich, Ltd.), accompanied by 10% fetal calf serum (FCS) and 1% penicillin and streptomycin (Sigma Aldrich, Ltd.), was added to 50 μl of 0.4% trypan blue solution(Sigma Aldrich, Ltd) to form a 1:2 dilution. This was repeated in four sixteen square chambers and the mean number of viable cells was obtained, and the Eq. (6) was applied.

$$Number of cells\ per\ ml = \left[\left(\frac{Total number of cells}{Number of squars counted} \right) \times 2 \right] \times 10^4 \quad (6)$$

2.6.2. Cell viability

The cell viability and number were both also discovered via colorimetric assay, in this case the 3-(4,5-dimethylthiazol-2-yl)-2,5-diphenyltetrazolium bromide (MTT) (Sigma Aldrich, Ltd) assay. The cells to be used for MTT assay were cultured in T25 tissue culture flask (25 cm^2) in the same manner as those that were used in other methods. When cells reached a high level of confluence (70–80% subconfluent), the cells were uncoupled from the flask surface via the use of 0.25% trypsin and 0.02% EDTA solution, after 5 to 15 min cells were then re-suspended and then counted by haemocytometer. After that the remained cell suspension mixture was pipetted into the wells of two separate 96-well micro plates each containing 100 μl of complete culture medium and the nylon based samples with a set cell density (5×10^4 cell/ml). Control samples containing the standard cell density and cell media and a separate blank which contained just culture media. The plates were then placed in an incubator set to 37.5° Celsius and 5% atmospheric CO_2.

After 24 h and 48 h respectively, the samples were removed from the incubator and placed into a biosafety cabinet. The complete media was removed and 50 μl of MTT reagent with a concentration of 5 mg per ml dissolved in media was added to the 96-well plate which had cells attached on the samples at the bottom of the well. The well plate was incubated for approximately 5 h out of direct sunlight to enable the MTT reagents to pass into the cells themselves and seat itself within the mitochondria where it was reduced to insoluble formazan, which turns purple. After the MTT reagent was then removed using a micro pipette and 100 μl of Dimethyl sulfoxide (DMSO) (Sigma Aldrich, Ltd) was added to cells to dissolve the purple formazan product. At this point optical density of the dissolved formazan was measured using a 96-well micro plate reader (FLUOstar OPTIMA Microplate Reader, Germany) with a wavelength of 570 nm. The average values for the three readings of each sample were averaged to produce a single value. The optical density of the solution was used as a measure of the cell viability or the living cell count.

3. Results and discussion

4.1 Topography.

Following CO_2 laser irradiation of the samples it is known that the sample surfaces would have risen in temperature and melted, corresponding to the thermolytic nature of the CO_2 laser-material interaction [29]. As melting was observed with the CO_2 laser processed samples, it is reasonable to state that the induced temperature rise following the laser-material interaction was above the nylon melting temperature of 262 °C [31]. As a result of this, scanning a predetermined pattern across the nylon 6,6 surfaces gave rise to a significant variation in topography when compared to the as-received sample (AR). This becomes more apparent when comparing the as-received sample (see Fig. 3(a)) with the laser patterned samples, the 3-D profiles of which are given in Fig. 3(b–e). From Fig. 3, it can be deduced that the CO_2 laser-induced patterned samples had considerably rougher surfaces with the largest peak heights being of the order of 44 μm in contrast to the as-received sample which had peaks heights of up to 0.5 μm. On account of the increase in

peak heights over the CO_2 laser-patterned samples the surface roughness (see Table 1) increased considerably with the largest Sa of 4.4 μm and the largest Ra of 2.2 μm being achieved with the 50 μm trench sample (CT50). It is given in Table 1 that the patterned samples with scan dimensions of 50 μm (samples CT50 and CH50) have larger Sa roughness values when compared to the samples patterned with 100 μm scan dimensions (samples CT100 and CH100). This can be attributed to the fact that the 50 μm scan dimensions irradiated more of the sample giving rise to an increase of mass being melted and re-solidified. Also, it can be seen from the Table 1 that the roughness for the hatch patterns had decreased in comparison to the trench patterns. This can be explained by the laser re-melting sections of the nylon 6,6 surface owed to the scanning process of the system. By re-melting these sections the material could then have re-solidified into a smoother surface topography. (see Table 1)

One factor of significance is that of the spot size on the surface of the material. That is, the beam spot size was 95 μm and consequently allowed the scans to overlap and thus eliminated the natural periodicity of the original scanned pattern. This could also allow one to explain the surface Sa roughness increase as seen in Table 1 as the scanned 50 μm dimensioned patterns (samples CT50 and CH50) had up to a several times larger Sa value compared to the 100 μm scan dimensioned nylon 6,6 samples (samples CT100 and CH100). That is, on account of significantly more melting and re-solidification taking place, on account of the overlapping, a rougher surface could have resulted.

Another aspect to consider is that of the sample surface area coverage as the laser beam was scanned across the nylon 6,6 samples. Owed to the spot size of the laser beam, Table 2, gives the area coverage for each sample and the maximum energy transferred in to the samples during the laser-material interaction. Taking sample CH50 as an example, 81% of the sample's area was irradiated and taken above the melting temperature four times, 18% was molten twice and 1% of the area had double coverage. This re-melting, as the laser beam was scanned across the surface, is likely to have had a significant impact upon the re-solidification process. For instance, the highest Sa roughness of 4.4 μm obtained from sample CT50 had a single area coverage of 10% and a double area coverage of 90%. When comparing this with sample CH50, which had mostly triple and quadruple area coverage, the surface roughness differed considerably. That is, for sample CH50 the Sa roughness was lower at 2.8 μm and can be attributed to the discrete melting and re-melting of the sample following the multiple passes of the laser beam. This will have likely eradicated the initial scanned pattern for sample CH50, making the sample smoother compared to sample CT50. This is further evidenced by the 3-D profiles shown in Fig. 3.

3.1. Surface chemical analysis

XPS was used to investigate any changes in the surface chemistry and composition of the nylon test samples as a result of the laser treatment. Scans were made over the whole binding energy range of interest, and high resolution scans were made over the C1s, O 1s and N 1s lines from the as-received and the laser-treated surfaces. The results of quantification of the data are shown in Table 3.

All samples showed approximately 10–11 atom % N, approximately 5–10 atom % O and approximately 80 atom % C. The lowest levels of O and N, and the highest level of C, was seen on the as-received (untreated) sample. This sample also showed the highest proportion of minor species typically associated with low levels of surface contamination as a result of handling, contact with packaging materials, etc. The total levels of surface contamination species including Na, S, Si, Cl, K and Mg were seen to reduce with increasing intensity of laser treatment, as shown in Fig. 4. The error bars in Fig. 4 are derived using the method of Harrison and Hazell [32] as implemented in CasaXPS v2.3.16. These low levels detected indicate a level of contamination at the monolayer level only.
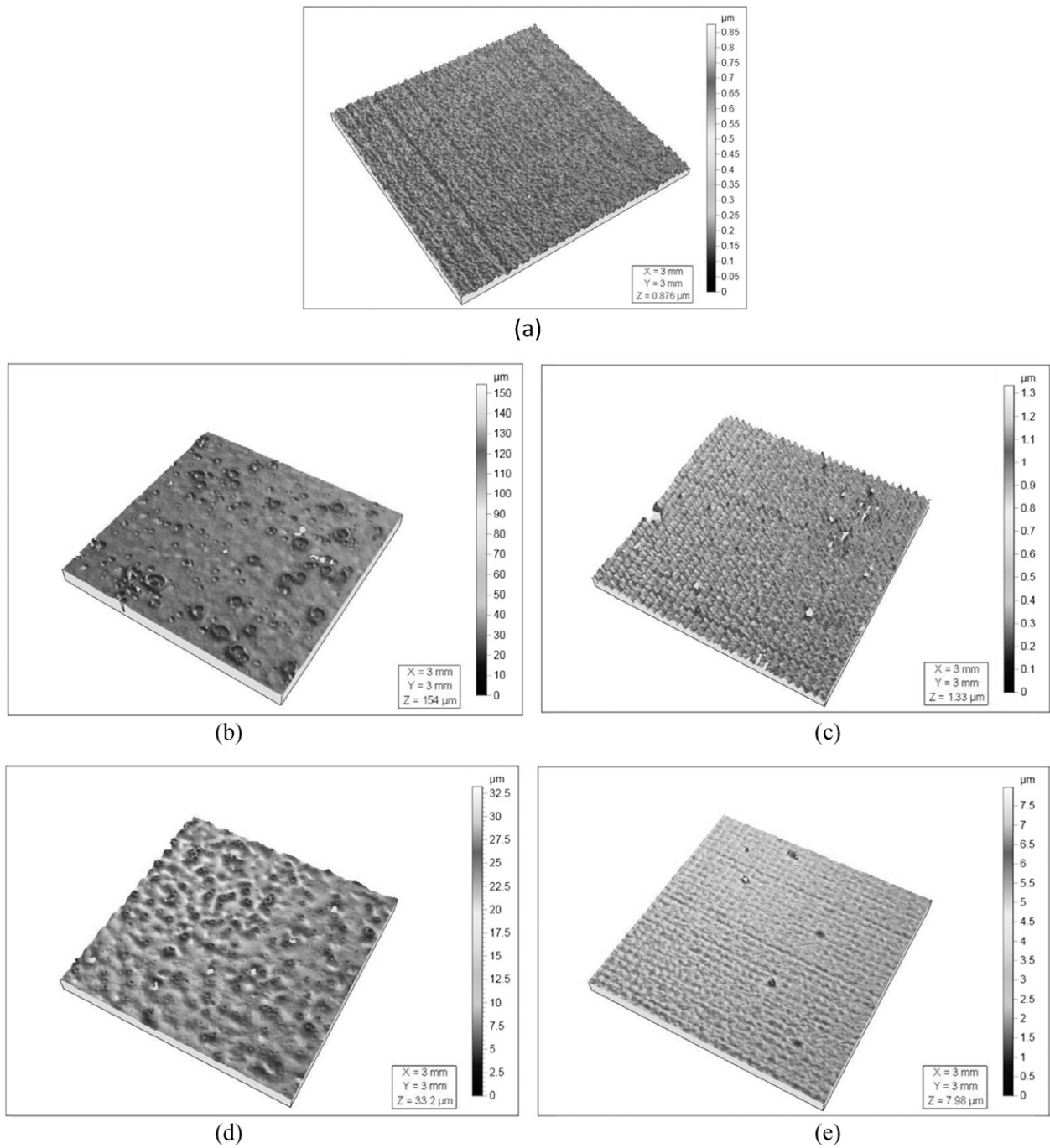
(a)

(b)

(c)

(d)

(e)

Fig. 3. 3-D profiles for the (a) as-received (b) CT50 (c) CT100 (d) CH50 and (e) CH100 samples.

The C 1s, O 1s and N 1s photoelectron lines are shown for the as-received sample and the treated sample, CT50, in Fig. 5. The spectra from the CH50, CH100 and CT100 samples were very similar to that shown here for the CT50 sample. The C 1s and N 1s spectra from the CT50 laser treated sample agree well with XPS spectra from pure and clean nylon reference material [33]. In these spectra, the C 1s spectrum

Table 1
Table showing the contact angle and the corresponding surface free energy for each sample.

Sample	Sa (μm)	Ra (μm)	Contact angle (°) water	Contact angle error (°) water	Surface energy (mJ m^{-2})
AR	0.097	0.023	56.36	1.29	49.12 ± 0.55
CT50	4.400	2.230	60.27	1.72	47.59 ± 0.44
CT100	0.201	0.115	55.24	0.81	47.16 ± 0.42
CH50	2.830	0.798	54.68	1.06	48.77 ± 0.45
CH100	0.236	0.080	57.38	0.61	52.18 ± 1.22

Table 2
Table giving the area coverage of the laser beam as it scans the patterns across the target material with the associated energy that is delivered for each sample.

Sample I.D.	Single area coverage	Double area coverage	Triple area coverage	Quadruple area coverage	Un-treated area	Energy (J)
CT50	10%	90%	0%	0%	0%	2333
CT100	95%	0%	0%	0%	5%	1167
CH50	0%	1%	18%	81%	0%	4667
CH100	9.5%	90.25%	0%	0%	0.25%	2333

Table 3
Results of surface composition analysis by XPS, in atom % excluding H.

Name	Surface composition (atom %)				
	AR	CT50	CH50	CT100	CH100
Na 1s	0.4	0.03	0.09	0.01	0.05
O 1s	10.4	11.3	10.8	10.6	10.5
N 1s	5.3	9.7	9.3	9.1	9.6
C1s	82.2	78.3	79.0	79.2	78.4
S 2p	0.6	0.06	0.06	0.2	0.1
Si 2p	0.5	0.4	0.5	0.6	0.4
Cl 2p	0.1	0.08	0.2	0.4	1.0
K 2s	0.3				
Mg 2 s	0.3	0.1	0.2		

shows (1) C—C bonding at approximately 285 eV corresponding to carbon in the CH_2 groups of the nylon backbone, (2) a component at approximately 286 eV corresponding to carbon in C—N bonds, and (3) a component at approximately 288 eV due to carbon in the nylon amide groups, —C(=O)N—. The equivalent C 1s spectrum from the as-received sample shows similar features but with reduced intensity relative to the C—C component at 285 eV, and with a further low intensity component at approximately 289.3 eV attributed to surface acid groups. Both the as-received and the CT50 samples showed O 1s spectra with a main component at approximately 531.3 eV due to oxygen in O=C bonds, as expected for Nylon. Both also showed a second component at approximately 533.1 eV, attributed to oxygen in surface acid groups. This second component was much weaker in the case of the treated samples. Both treated and as-received samples showed an N 1s peak at approximately 399.6 eV, in agreement with expected values for Nylon.

The XPS data suggests that the effect of laser treatment was to remove surface contamination from the surfaces, resulting in spectra exhibiting composition and chemical state information in good agreement with established XPS reference spectra for Nylon [33]. This cleaning effect may have been by evaporation or sublimation, or possibly as a result of melting and subsequent solidification of the outermost surface layers accompanied by migration of any surface contaminant species away from the surface. The laser treatment did not appear to cause any local chemical degradation of the molecular structure of the Nylon.

3.2. Wettability analysis

When analysing the contact angle in relation to the surface free energy for each sample, it can be seen from Table 1 that three different types of trend were identified. The first trend refers to sample CT100, where the slight reduction in contact angle of approximately 1°, θ, from the CO_2 laser treatment was brought about by a slight increase in the surface free energy of the sample. This indicated a very small

Table 4
Results showing statistical significance of the stem cell results.

Pairwise Comparisons						
(I) Time	(J) Time	Mean difference (I-J)	Std. Error	Sig.[a]	95% confidence interval for difference[a]	
					Lower Bound	Upper Bound
1	2	− 13.941[*]	2.066	0.000	− 19.340	− 8.543
	3	− 19.759[*]	2.502	0.000	− 26.295	− 13.222
2	1	13.941[*]	2.066	0.000	8.543	19.340
	3	− 5.817	2.338	0.065	− 11.925	0.291
3	1	19.759[*]	2.502	0.000	13.222	26.295
	2	5.817	2.338	0.065	− 0.291	11.925

Based on estimated marginal means.

[*] .The mean difference is significant at the 0.05 level.

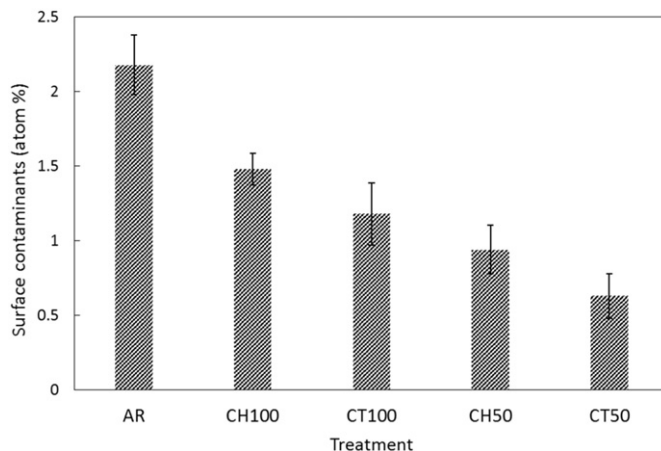[a] Adjustment for multiple comparisons: Bonferroni.

Fig. 4. Total overall atom % of surface contamination species on the as-received and laser treated surfaces, shown as a function of treatment. The error bars are derived using the method of Harrison and Hazell [32] as implemented in CasaXPS v2.3.16.

enhancement of adhesion characteristics for sample CT100, if any. The second trend refers to sample CH100, whereby the laser treatment brought about an increase of the contact angle (approximately 1°) which was a result of the increase in the surface free energy. The third trend refers to the samples with a 50 μm spacing, CT50 and CH50, whereby the surface free energy decreased for each sample even though the contact angle increased for sample CT50 (approximately 4°) and decreased for sample CH50 (approximately 2°), compared to the as-received sample. These three trends show that CO_2 laser surface treatment can be employed to make discrete changes to both the contact angle and the surface free energy, through topography and surface chemistry modification, to discretely modulate the adhesion characteristics.

The discrete changes in wettability characteristics brought about by the CO_2 laser surface treatment are in contrast with what has been observed by others for laser patterning of polyamide 6,6, where a significant increase of θ was reported [11]. This may be due to this particular CO_2 laser surface treatment giving rise to discrete changes in surface topography (see Table 1 and Fig. 2) and surface chemistry (see Table 3) when compared to previous experimentation. This is significant as any treated polymeric samples for use as a platform for the growth of biological cells needs to be enhanced, free from the generation of toxic surfaces [34]. In addition to this, those variations in contact angles between the samples may likely be related to the existence of a mixed-state regime, as it has been found in literature for similar laser processing applications [26,27,35]. Having said that, even though the wettability characteristics modifications were very discrete, appearing to have little change on the adhesion characteristics, it will be seen from the MSC response that the biological adhesion properties of the CO_2 laser surface treated nylon 6,6 was significantly enhanced.

3.3. Mesenchymal stem cell response

The MSCs grown on the blank samples grew noticeably over 48 h as opposed to 24 h. It should also be noted that all samples that were grown on nylon 6,6 samples grew considerably better than the blanks which were grown in the absence of nylon 6,6. The CO_2 laser treated nylon 6,6 samples all grew better in terms of viable cell count than their as-received counterpart (see Fig. 6 and Fig. 7). As one can see from Fig. 6, absorbance was highest under the CH50 sub group. In the CH50 sub group the 48 h absorbance was higher than the 24 h samples, a theme that was repeated in both the blank, AR and CT100 group. In the CT50 and the CH100 group the 24 h absorbance was slightly higher than the 48 h absorbance; however the values received were close in both these groups. This observed increase in cell viability could have been a
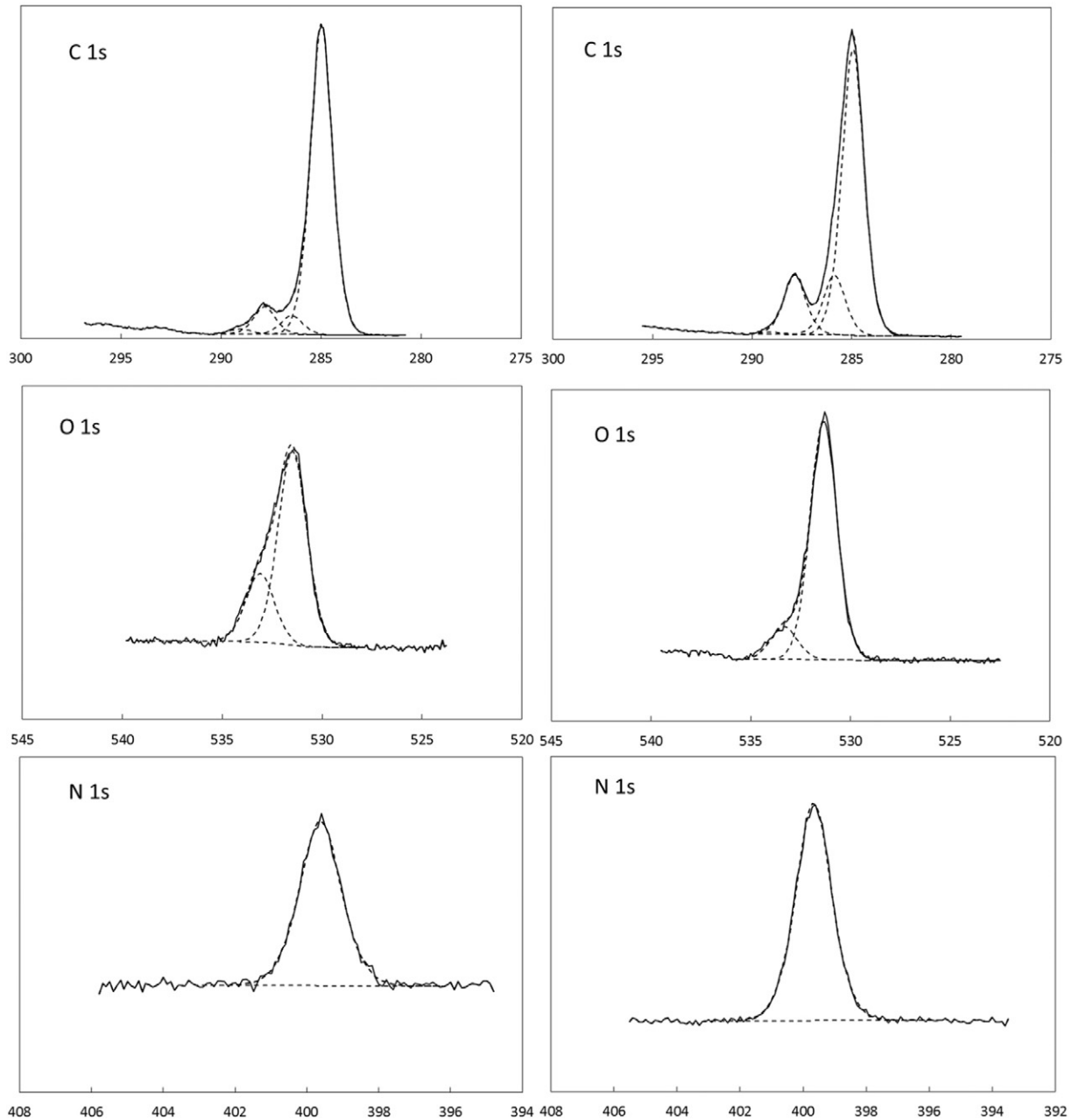
Fig. 5. From top, C 1s, O 1s and N 1s spectra for the as-received (left) and CT50 treated surfaces (right).

result of the increase in surface roughness and slight increase in O1s content (see Fig. 8), eliciting a more enhanced response from the MSCs. This is in accordance with other researchers in the field who have shown that cells can be manipulated by variations in surface properties [9,36–39].

As shown in Fig. 7, in the majority of cases, the number of MSCs increased over time in the presence of the CO_2 laser treated Nylon samples. The manner of reaction seen in the cells themselves was variable depending on the processing parameters used. The 24 h MSC count results were generally lower than those seen at the longer incubation time of 48 h. This is due to the fact that when cells are seeded onto a surface, MSCs go through a lag phase before entering the growth phase. In the vast majority of samples all readings were higher than those found in the control sample, as well as this, incubation over time also yielded higher readings, as was to be expected. In addition to this, Table 4 shows that there was a significant difference between the 24 h time course and the 48 h ($p < 0.05$).

It has been previously shown that increased roughness characteristics can result in increased cell adhesion and conversely smoother surfaces result in cell spreading [40]. In comparison with the work conducted here, there seemed to be very little variation in cell spreading; however, an increase in cell adhesion and subsequent enhancement of MSC growth was apparent, following CO_2 laser surface treatment. This could be due to the discrete surface modification nature arising from the CO_2 laser surface treatment, compared to alternative techniques. Another aspect shown in the literature on a number of occasions to have a beneficial effect on a variety of cellular processes in-vivo is that of surface chemistry modification [41]. That being said, the efficacy of this method of modifying is dependent on specific processing parameters, as a result it could be beneficial to process materials purely in the presence of atmospheric conditions present, more research is required into this specific parameter. Work by Wan et al. 2010 [42] highlighted the beneficial nature of the presence of biomaterials that contain an above average proportion of nitrogen atoms. The article
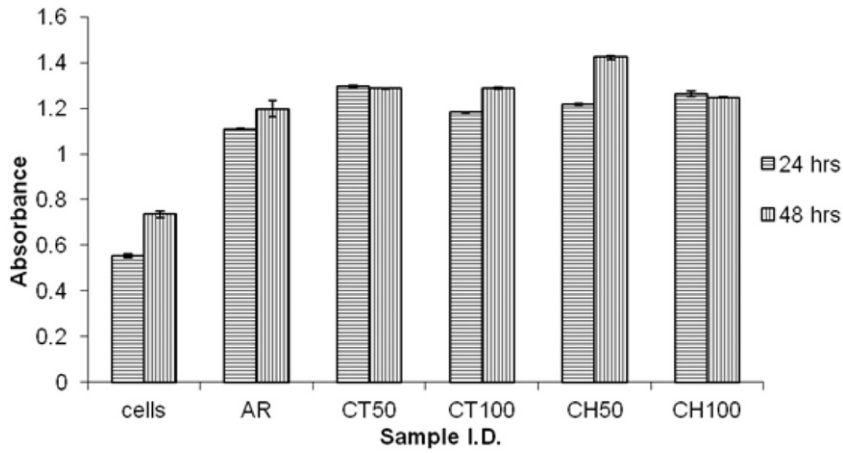
Fig. 6. Viability MTT absorbance results for each sample.

discusses the enhanced biocompatibility displayed by high nitrogen products compared to materials with a lower nitrogen content. As well as this, the article discusses the decreased coagulation time and an enhanced and modulated wettability. This is significant as an increase in nitrogen content on the surface, along with an increase in surface roughness, enhanced the MSC response within this work with
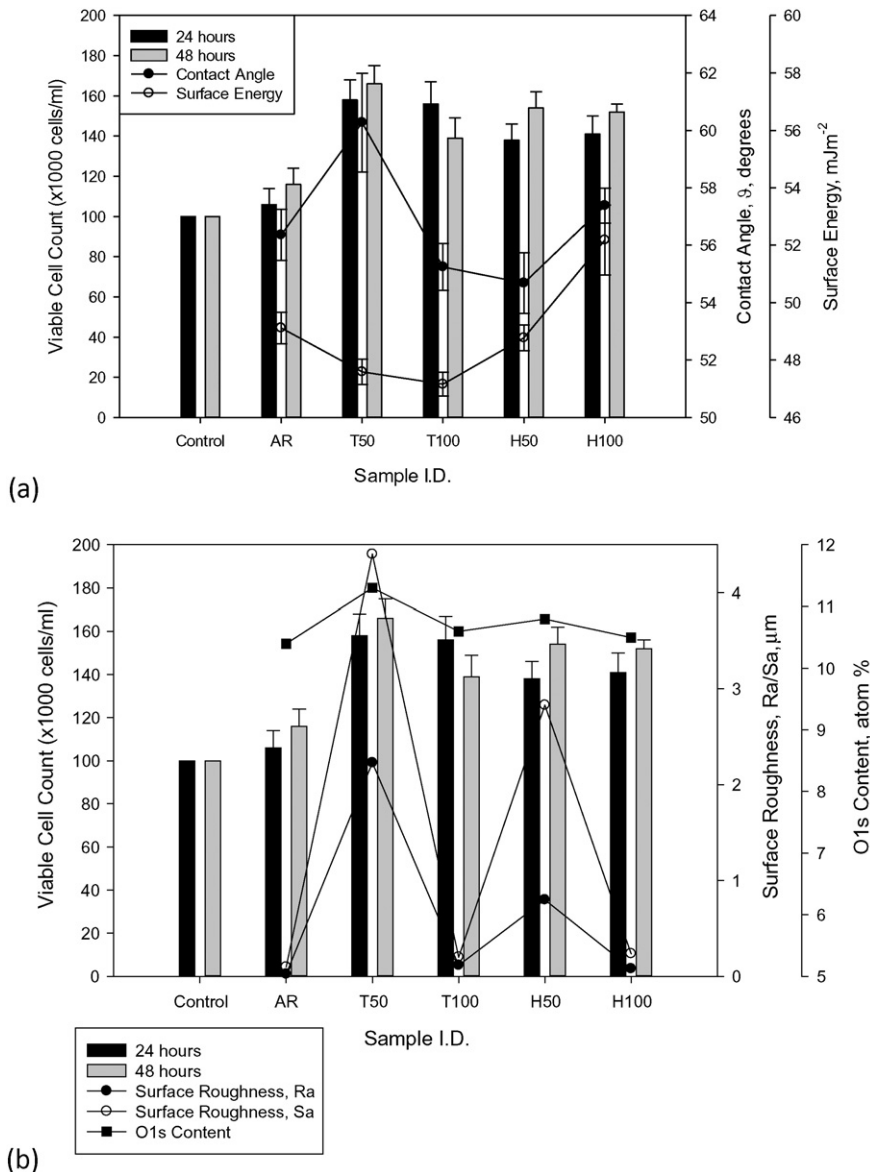

(a)

(b)

Fig. 7. Viable cell count for each sample following 24 h and 48 h of incubation time in relation to (a) the contact angle and surface energy and (b) the surface roughness and O1s content.
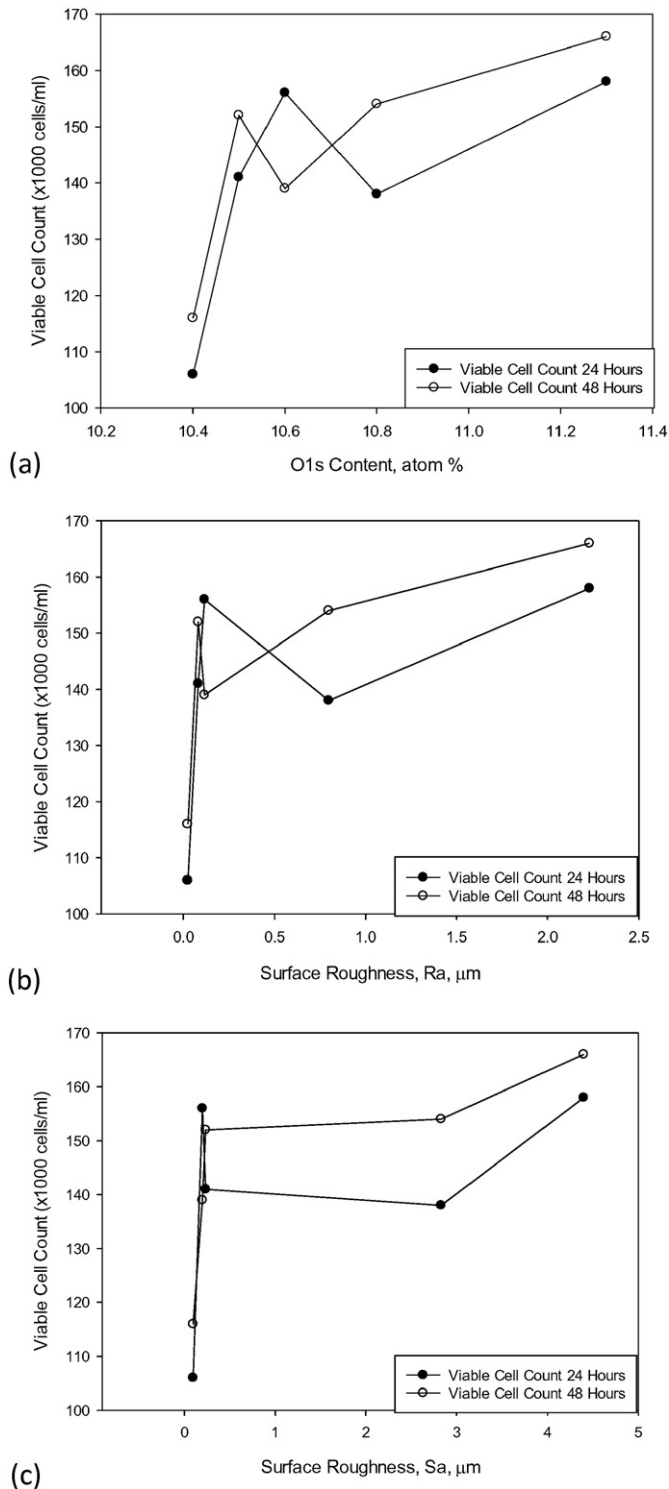
Fig. 8. Graphs of MSC viable cell count against (a) O1s content, (b) Ra surface roughness and (c) Sa surface roughness for all samples.

enhancement in MSC growth, there has been no evidence to suggest that there is a correlation between the promotion of viable MSCs and the laser-modified contact angle/surface energy (see Fig. 6(a)).

In addition to the increase in cell viability it should also be noted that in some instances it was observed that the CO_2 laser treated nylon 6,6 samples gave rise to some form of directional growth, especially following 24 h of incubation (see Fig. 9). That is, for the trench patterned samples it was seen that the MSCs seemed to preferentially grow in the direction of the parallel line scanned pattern. This highlights that this particular surface modification technique could provide discrete surface parameter variation to promote directional MSC growth. Although, further investigations are needed to ascertain the extent of this promotional growth in accordance with others in the field [45,46].

4. Conclusions

Through discrete CO_2 laser surface treatment it has been shown that small, discrete modifications in the surface topography and surface chemistry can be brought about in nylon 6,6. That is, by using a simple but effective parallel line and hatch pattern, a CO_2 laser can inhibit increases in surface roughness of up to 4 μm and can give rise to variations in surface chemistry with low increases (up to 1 atom %) in O1s content. These discrete changes in surface properties have ultimately given rise
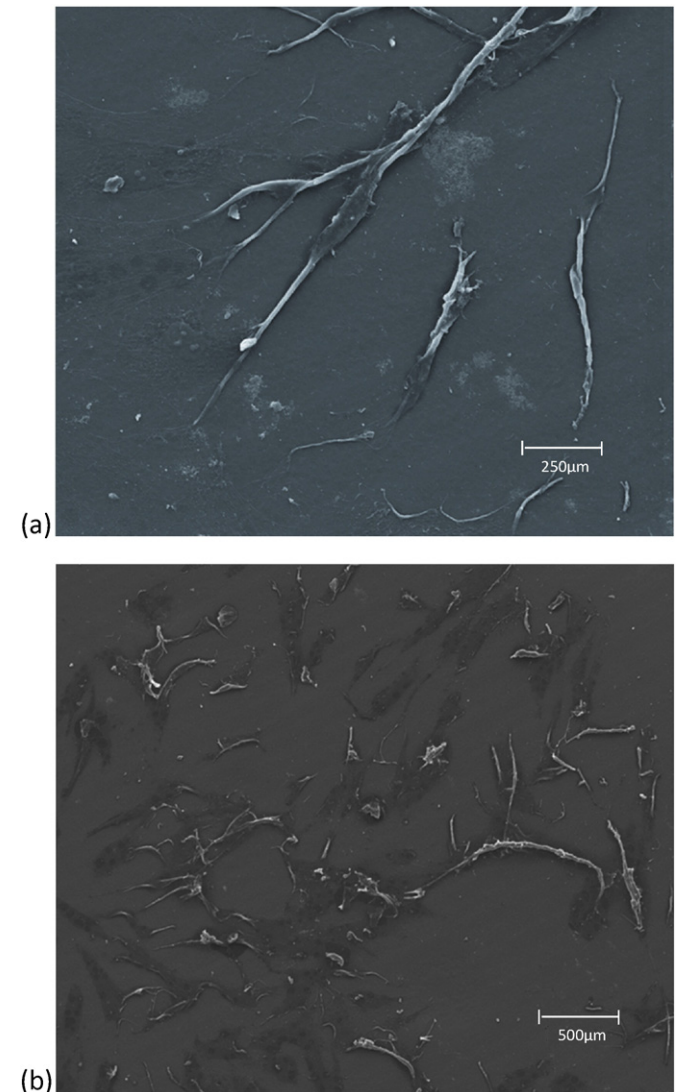

Fig. 9. SEM micrographs of MSC growth on (a) Sample CT100 and (b) Sample CH100 following 24 h of incubation.

regards to viable MSC count (see Fig. 7). It should also be noted that from the literature, an increase in oxygen content available at the surface resulted in an increased level of healing and bone implant interaction [43].

It has been shown repeatedly in literature that the wettability has an effect on cell adhesion. Backakova et al. [44] reported that an optimum wetting angle exists for an individual surface and that this can be used as a guide line for cellular response and has a beneficial effect on cellular behaviour. Whilst the CO_2 laser surface treatment did give rise to an

to a small modification in the wettability characteristics with contact angles between 54° and 60° being observed. This directly correlated with surface energies between 47 mJ m^{-2} and 53 mJ m^{-2}.

Although the surface property modifications were discrete, it was identified that the CO_2 laser surface treatments gave rise to an increase in mesenchymal stem cell (MSC) viable cell number (up to 60,000 cells/ml) following 24 h and 48 h of incubation. What is more, the CO_2 laser surface treatment gave rise to directional cell growth which could be easily implemented for applications which require biological cells to grow in a specific area on the material.

As the ageing world population is being required to work longer in a lifetime, the need is ever increasing for new technologies which can meet demand on a pharmaceutical scale. On account of the ease of automation and scale up of this CO_2 laser surface treatment technique, it is an extremely attractive means for modifying polymeric materials which can act as platforms for the manipulation and enhancement of stem cell growth.

References

[1] R.S. Benson, Use of radiation in biomaterials science, Nucl. Instrum. Methods Phys. Res., Sect. B 191 (2002) 752–757.
[2] F. Arefi-Khonsari, M. Tatoulian, F. Bretagnol, O. Bouloussa, F. Rondelez, Processing of polymers by plasma technologies, Surf. Coat. Technol. 200 (2005) 14–20.
[3] D. Pappas, A. Bujanda, J.D. Demaree, J.K. Hirvonen, W. Kosik, R. Jensen, et al., Surface modification of polyamide fibers and films using atmospheric plasmas, Surf. Coat. Technol. 201 (2006) 4384–4388.
[4] E.M. Harnett, J. Alderman, T. Wood, The surface energy of various biomaterials coated with adhesion molecules used in cell culture, Colloids and Surfaces B. 55 (2007) 4970–4980.
[5] A.C. Popa, G.E. Stan, M. Enculescu, C. Tanase, D.U. Tulyaganov, J.M. Ferreira, Superior biofunctionality of dental implant fixtures uniformly coated with durable bioglass films by magnetron sputtering, J. Mech. Behav. Biomed. Mater. 51 (2015) 313–327.
[6] M.F. Cutiongco, D.E. Anderson, M.T. Hinds, E.K. Yim, In vitro and ex vivo hemocompatibility of off-the-shelf modified poly(vinyl alcohol) vascular grafts, Acta Biomater. 25 (2015) 97–108.
[7] T.Y. Lo, Y.J. Wang, D.M. Liu, W.T. Whang, Surface characteristics and biofunctionality of a novel high-performance, hydrophilic Jeffamine-added fluoro-containing polyimide for biomedical applications, J. Polym. Res. 22 (2015) 4.
[8] W.M. Steen, K.G. Watkins, J. Mazumder, Laser Material Processing, fourth ed. Springer, UK, 2010.
[9] D.G. Waugh, J. Lawrence, Laser Surface Treatment of a Polymeric Biomaterial, Old City Publishing, Philadelphia, USA, 2013.
[10] D.G. Waugh, J. Lawrence, Laser Surface Engineering: Processes and Applications, Elsevier Ltd, Cambridge, UK, 2015.
[11] K.L. Mittal, T. Bahners, Laser Surface Modification and Adhesion, Wiley-Scrivener, USA, 2014.
[12] M. Makropoulou, A.A. Serafetinides, C.D. Skordoulis, Ultra-violet and infra-red laser ablation studies of biocompatible polymers, Lasers in Medical Science. 10 (1995) 201–206.
[13] H. Koga, L. Engebretsen, J.E. Brinchmann, T. Muneta, I. Sekiya, Mesenchymal stem cell-based therapy for cartilage repair: a review, Knee Surg. Sports Traumatol. Arthrosc. 17 (2009) 1289–1297.
[14] E.T. Stace, S.G. Dakin, P.A. Mouthuy, A.J. Carr, Translating regenerative biomaterials into clinical practice, J. Cell. Physiol. 231 (2016) 36–49.
[15] W. Wang, K. Kratz, M. Behl, W. Yan, Y. Liu, X. Xu, et al., The interaction of adipose-derived human mesenchymal stem cells and polyether ether ketone, Clin. Hemorrheol. Microcirc. 61 (2015) 301–321.
[16] M.G. Angelos, D.S. Kaufman, Pluripotent stem cell applications for regenerative medicine, Curr. Opin. Organ Transplant 20 (2015) 663–670.
[17] W. Wang, K. Kratz, M. Behl, W. Yan, Y. Liu, X. Xu, et al., The interaction of adipose-derived human mesenchymal stem cells and polyether ether ketone, Clin. Hemorrheol. Microcirc. 61 (2015) 301–321.
[18] L.L. Meisner, A.I. Lotkov, V.A. Matveeva, L.A. Artemieva, S.N. Meisner, A.L. Matveev, Effect of silicon, titanium, and zirconium ion implantation on NiTi biocompatibility, Adv. Mater. Sci. Eng. 2012 (2012) 1–16.
[19] H. Koga, L. Engebretsen, J.E. Brinchmann, T. Muneta, I. Sekiya, Mesenchymal stem cell-based therapy for cartilage repair: a review. Knee surgery, sports traumatology, arthroscopy, Official Journal of the ESSKA. 17 (2009) 1289–1297.
[20] S. Myllymaa, E. Kaivosoja, K. Myllymaa, T. Sillat, H. Korhonen, R. Lappalainen, Y.T. Konttinen, Adhesion, spreading and osteogenic differentiation of mesenchymal stem cells cultured on micropatterned amorphous diamond, titanium, tantalum, and chromium coatings on silicon, J. Mater. Sci. Mater. Med. 21 (2010) 329–341.
[21] D.S. Kommireddy, S.M. Sriram, Y.M. Lvov, D.K. Mills, Stem cell attachment to layer-by-layer assembled TiO2 nanoparticle thin films, Biomaterials 27 (2006) 4296–4303.
[22] A.S. Curtis, C.D. Wilkinson, Reactions of cells to topography, J. Biomater. Sci. Polym. Ed. 9 (1998) 1313–1329.
[23] E.K. Yim, S.W. Pang, K.W. Leong, Synthetic nanostructures inducing differentiation of human mesenchymal stem cells into neuronal lineage, Exp. Cell Res. 313 (2007) 1820–1829.
[24] J. Li, Y. Dou, J. Yang, Y. Yin, H. Zhang, F. Yao, et al., Surface characterization and biocompatibility of micro- and nano-hydroxyapatite/chitosan-gelatin network films, Mater. Sci. Eng. C 29 (2009) 1207–1215.
[25] T.P. Kunzler, C. Huwiler, T. Drobek, J. Voros, N.D. Spencer, Systematic study of osteoblast response to nanotopography by means of nanoparticle-density gradients, Biomaterials 28 (2007) 5000–5006.
[26] D.G. Waugh, J. Lawrence, Wettability and osteoblast cell response modulation through UV laser processing of nylon 6,6, Appl. Surf. Sci. 257 (2011) 8798–8812.
[27] D.G. Waugh, J. Lawrence, D.J. Morgan, C.L. Thomas, Interaction of CO2 laser-modified nylon with osteoblast cells in relation to wettability, Mater. Sci. Eng. C 29 (2009) 2514–2524.
[28] D.G. Rance, Chapter 6 - thermodynamics of wetting: From its molecular basis to technological application, in: D.M. Brewis (Ed.), Surface Analysis and Pretreatment of Plastics and Metals, Applied Science Publishers, UK, 1982.
[29] Allmen, M.V. Laser-beam Interactions with Materials. Bern, Germany, Springer, 1995.
[30] M.P. Seah, S.J. Spencer, Repeatable intensity calibration of an X-ray photoelectron spectrometer, J. Electron Spectrosc. Relat. Phenom. 151 (2006) 178–181.
[31] R. Palazzetti, A. Zucchelli, C. Gualandi, M.L. Focarete, L. Donati, G. Minak, et al., Influence of electrospun Nylon 6,6 nanofibrous mats on the interlaminar properties of Gr–epoxy composite laminates, Compos. Struct. 94 (2012) 571–579.
[32] K. Harrison, L.B. Hazell, The determination of uncertainties in quantitative XPS/AES and its impact of data acquisition strategy, Surf. Interface Anal. 18 (1992) 368–376.
[33] G. Beamson, D. Briggs, High Resolution XPS of Organic Polymers: The Scienta ESCA 300 Database, John Wiley & Sons, Chichester, 1992.
[34] D.G. Waugh, J. Lawrence, E.M. Brown, Osteoblast cell response to a CO2 laser modified polymeric material, Opt. Lasers Eng. 50 (2012) 236–247.
[35] M.J. Dutta, I. Manna, Laser-assisted Fabrication of Materials, Springer-Verlag, Berlin Heidelberg, 2013.
[36] A.S.G. Curtis, C.D.W. Wilkinson, Reactions of cells to topography, J. Biomater. Sci. Polym. Ed. 9 (1998) 1313–1329.
[37] L. Hao, J. Lawrence, Laser Surface Treatment of Bio-implant Materials, John Wiley & Sons Inc., New Jersey, USA, 2005.
[38] H. Mirzadeh, M. Dadsetan, Influence of laser surface modifying of polyethylene terephthalate on fibroblast cell adhesion, Radiat. Phys. Chem. 67 (2003) 381–385.
[39] W. Pfleging, M. Bruns, Laser-assisted modification of polystyrene surfaces for cell culture applications, Appl. Surf. Sci. 253 (2007) 9177–9184.
[40] E. Biazar, M. Heidari, A. Asefnezhad, N. Montazeri, The relationship between cellular adhesion and surface roughness in polystyrene modified by microwave plasma radiation, International Journal of Medicine. 6 (2011) 631–639.
[41] J.C. Carrero-Sanchez, A.L. Elias, R. Mancilla, G. Arrelin, H. Terrones, J.P. Laclette, M. Terrones, Biocompatibility and toxicological studies of carbon nanotubes doped with nitrogen, Nano Lett. 6 (2006) 1609–1616.
[42] P. Wan, Y. Ren, B. Zhang, K. Yang, Effect of nitrogen on blood compatibility of nickel-free high nitrogen stainless steel for biomaterial, Mater. Sci. Eng. C 30 (2010) 1183–1189.
[43] R.S. Faeda, H.S. Tavares, R. Sartori, A.C. Guastaldi, E. Marcantonio, Jr. evaluation of titanium implants with surface modification by laser beam.Biomechanical study in rabbit tibias, Brazilian Oral Research. 23 (2009) 137–143.
[44] L. Backakova, E. Filova, M. Parizek, T. Ruml, T. Svorcik, Modulation of cell adhesion, proliferation and differentiation on materials designed for body implants, Biotechnol. Adv. 29 (2011) 739–767.
[45] H. Aubin, J.W. Nichol, C.B. Hutson, H. Bae, A.L. Sieminski, D.M. Cropek, et al., Directed 3D cell alignment and elongation in microengineered hydrogels, Biomaterials 31 (2010) 6941–6951.
[46] J.J. Norman, T.A. Desai, Control of cellular organization in three dimensions using a microfabricated polydimethylsiloxane-collagen composite tissue scaffold, Tissue Eng. 11 (2005) 378–386.